Appl. Phys. B 70, 211–217 (2000) / Digital Object Identifier (DOI) 10.1007/s003409900098

Applied Physics B
Lasers
and Optics

Spatial characteristics of K_α radiation from weakly relativistic laser plasmas

D.C. Eder*, G. Pretzler, E. Fill, K. Eidmann, A. Saemann

Max-Planck-Institut für Quantenoptik, D-85748 Garching, Germany

Received: 6 April 1999/Revised version: 31 May 1999/Published online: 11 August 1999

Abstract. The spatial dependence of K_α emission generated from laser-produced hot electrons is investigated experimentally and theoretically. In addition, the conversion efficiency of K_α production as a function of laser intensity is measured and compared with modeling results. We use the terawatt Ti:sapphire laser at MPQ and vary the peak intensity from 10^{15} to 10^{18} W/cm^2 with a pulse duration of 200 fs. A solid Cu target is placed at various positions in the laser focus, which allows one to vary the intensity but keep the total energy on the target constant. When the target is near best focus, the FWHM of the K_α emission, measured using a knife-edge, is considerably larger than the FWHM of the laser intensity. In measuring the efficiency of K_α production using the fundamental wavelength of the laser, a clear maximum of K_α emission is observed at a position away from best focus, where the peak intensity is down by more than an order of magnitude from the value at best focus. When the second harmonic of the laser is used, the K_α emission is peaked near best focus. The K_α emission from layer targets is used to obtain an estimate of the temperature of the hot electrons. Modeling of K_α production, using a Monte Carlo electron/photon transport code, shows the relationship between incident electron energy and the emitted K_α emission. Efficient K_α generation from the low-intensity wings of the laser pulse contributes to the large spot size of the K_α emission. The lower electron temperatures that are expected for the second harmonic explain the differences in the location of maximum K_α emission for the two wavelengths. We discuss the use of K_α emission in photoionizing inner-shell electrons with the goal of achieving X-ray lasing at short wavelengths.

PACS: 52.40.Nk; 52.60+h; 52.70.La

Ultrashort laser pulses [1–3] incident on solid or gas targets can produce hot electrons. When these hot electrons enter solid material, bremsstrahlung and characteristic X-ray radiation are produced. The spectra of X-ray emission produced by ultrashort laser pulses have been measured by many laboratories [4–6]. For mid-Z materials, the generation of K_α photons is of particular interest. Over a range of laser conditions, the K_α emission can dominate the spectrum in the few keV range. This source of X-rays (8 keV for Cu K_α) is a potential pump source for an inner-shell photoionized X-ray laser [7–12]. Prior to designing an X-ray laser based on this pump source, it is necessary to understand the emission of K_α as a function of the laser conditions.

The energy spectrum of hot electrons generated by ultrashort laser pulses is usually characteristic of a Boltzmann distribution with an effective temperature denoted as $T_{\rm hot}$. In some cases, two temperatures are used to characterize the spectrum [13]. Of particular interest is the scaling of $T_{\rm hot}$ with the intensity and wavelength of the driving laser. An early model of resonant absorption in a self-consistent sharp density gradient gives a scaling of [14]

$$T_{\rm hot} \sim (I\lambda^2)^{1/3}\,, \tag{1}$$

where I is the laser intensity and λ is the laser wavelength. In this model, a fraction of the laser energy is carried away by a free-streaming, low-density, high-energy electron component,

$$\alpha I = \beta n_{\rm hot} m v_{\rm hot}^3/2\,, \tag{2}$$

where α is the fraction of the incident flux absorbed by hot electrons; $v_{\rm hot}$ is the hot-electron thermal velocity $(T_{\rm hot}/m)^{1/2}$: $n_{\rm hot}$ is the hot-electron density; and β is a number of order unity characterizing the energy carried away by an almost Maxwellian distribution. In the modeling presented in this paper, we use this relationship assuming that α and β are independent of the laser intensity. A recent compilation of experiments has stated a scaling of $T_{\rm hot}$ with intensity and wavelength as $(I\lambda^2)^{1/3-1/2}$ [15]. Most current experiments and simulations have a scaling closer to $(I\lambda^2)^{1/3}$ than $(I\lambda^2)^{1/2}$. See, for example, [16]. In our modeling, we use $(I\lambda^2)^{1/3}$, but the results would not be made fundamentally different by using the $(I\lambda^2)^{1/2}$ scaling.

The spot size of K_α emission has been measured in the past for plasmas produced by ultrashort laser pulses. For $I\lambda^2$

*On leave from Lawrence Livermore National Laboratory, Livermore, CA 94550, USA

in the 10^{16} (W/cm^2)μm^2 range, the size of the K_α emission is of the order of the laser spot size [5]. For intensities in this range we obtain similar results. For higher intensities we observe the spot size of the K_α emission to be significantly larger than the laser spot size. When a prepulse is used, electrons produced by the laser can travel significant distances in the lateral direction and produce a large K_α spot. In the case of no prepulse, electrons can escape from the surface and re-enter the solid at a significant distance from the laser spot. The idea of hot electrons doing complex orbits is supported by an experiment that measured a relatively long pulse duration for K_α emission compared with the laser pulse duration [17]. In this paper, we discuss another contribution to a large K_α spot size associated with the low-intensity wings of the laser pulse.

Section 1 presents measurements of the spot size of K_α emission and the total amount of K_α emission as a function of target displacement from the location of best focus. In Sect. 2, we discuss a time-independent, coupled electron/photon Monte Carlo transport code. In Sect. 3, this code is applied to help explain our experimental measurements. Sect. 4 discusses the use of K_α emission as an X-ray laser pump source. In Sect. 5, we give our conclusions and plans for future experiments.

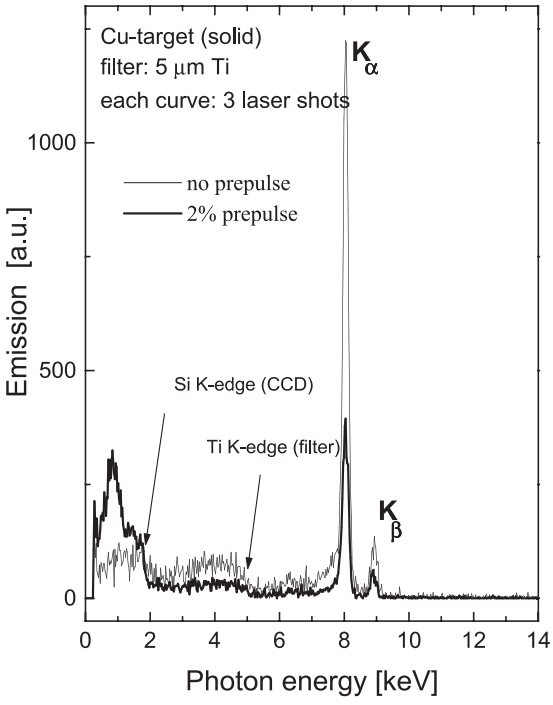

Fig. 1. Cu spectra using the fundamental wavelength with a prepulse and having "no prepulse"

1 Experiments

Experiments were done with 200-fs/200-mJ laser pulses from the 10-Hz ATLAS Ti:sapphire laser at Max-Planck-Institute of Quantum Optics. The 790-nm wavelength pulses were focused by an f/2.5 off-axis parabola to a peak intensity of 1.8×10^{18} W/cm^2. About 50% of the energy are contained in a spot of 10 μm diameter. An artificial prepulse could be introduced (with an energy of 4 mJ, 650 ps before the main pulse), but intrinsic prepulses and a pulse pedestal on the 10^{-4} level were always present and created a small plasma before the main pulse arrived on the target. For part of the experiment, pulses were frequency-doubled by a KDP crystal. These 395-nm pulses achieved energies of 70 mJ and had high contrast (10^{-6} at 1 ps before the maximum, 10^{-12} a few ns before the pulse), such that considerably less preplasma was generated as compared with the fundamental (for an assessment of the preplasma scale length L/λ for the different conditions see [18]).

Solid slabs were used as target, which were in rotation for positioning each laser shot on a fresh surface. The pulses were p-polarized and incident at 45°. Diagnostics was provided by a backside-illuminated thinned X-ray CCD observing the emission perpendicularly to the target surface. The CCD was used as a dispersionless spectrometer in the keV range. The principle of this technique is to detect single hard X-ray photons within single pixels of the CCD chip by using the fact that the signal delivered by the device (i.e. the number of charges produced) is strictly proportional to the incident photon energy. Clear hard X-ray spectra are obtained by this method if numeric event recognition techniques are applied. A calibrated CCD [19] is used for our experiments, and so quantitative spectra could be measured. The spectra show that the X-ray emission in the 1–10 keV range has strong Cu K_α and K_β radiation. When a prepulse is added there is strong L-shell radiation as well. Figure 1 shows spectra for Cu with and without an applied prepulse. Using appropriate filters suppresses the L-shell radiation so that the K-shell emission remained as the dominating part for both cases.

To determine the source size of the K-shell radiation, the distance from the target to the CCD is reduced so that the CCD is overexposed (i.e. most pixels multiply hit). The number of bremsstrahlung photons recorded by the CCD is less than 10% of the number of K_α photons. A knife-edge is positioned close to the target between it and the CCD to produce a magnification of 30. A Gaussian focal spot is assumed and the FWHM of the spot size is determined by evaluating the resulting half-shade images, the absolute number of photons being obtained as well. The spatial resolution of the knife-edge technique was 5 μm. The target is moved forward and backward in the focus, thus producing different laser intensity distributions on the target. This results in a peak intensity on the target in the 10^{15} to 10^{18} W/cm^2 range, with the total energy remaining constant.

We measure the FWHM of the K_α emission as a function of target displacement from best focus using an applied prepulse and with no applied prepulse. These data are shown in Fig. 2 along with the FWHM of the laser intensity. For the case of a prepulse, the K_α spot size is a factor of about 10 times larger than the laser spot size near the location of best focus. We believe that electrons generated in the extended preplasma can move significant distances in the lateral direction and thus produce a large K_α spot size. For the case of no applied prepulse, the K_α spot size is still a factor of about five larger than the laser spot size for target positions near best focus. While there can be a small intrinsic prepulse when the laser is operated at the fundamental wavelength, the preplasma is not expected to be large enough to explain the large spot size of K_α emission. One possible reason for a larger spot size is that the electrons can leave the surface of the ma-

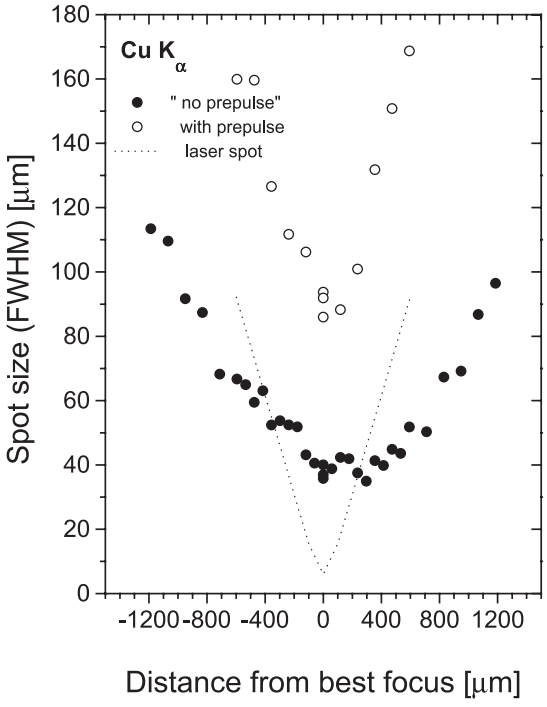

Fig. 2. The FWHM of the Cu K_α emission using a prepulse and having "no prepulse" as compared to the FWHM of the incident laser intensity. Negative values of the distance indicate that the focus is situated in front of the target. For positive values the focus is within the target

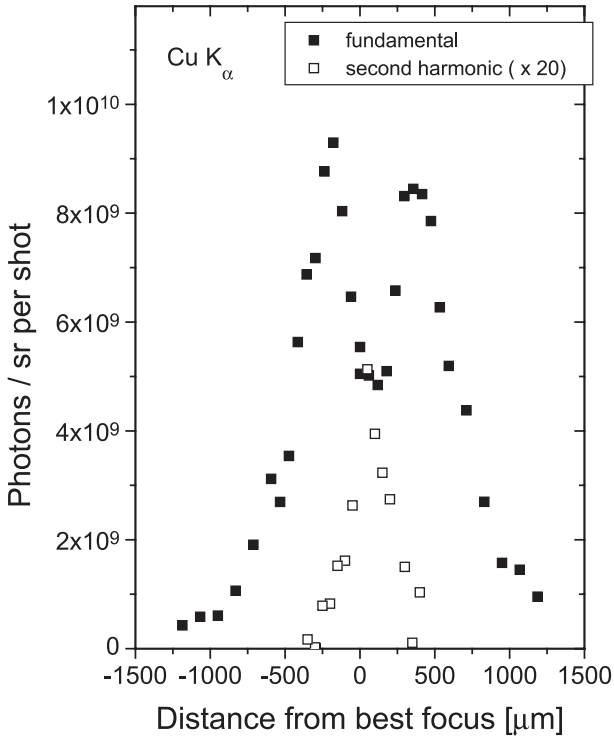

Fig. 3. The total amount of Cu K_α emission as a function of target displacement from location of best focus for the fundamental wavelength and the second harmonic. A number of 10^{10} photons/sr corresponds to an energy conversion efficiency into K_α of 2×10^{-4}. The results for the second harmonic are multiplied by a factor of 20. As in Fig. 2 negative values of the distance indicate a focus in front of the target

terial near the center of the laser spot and as they return to the surface due to electrostatic forces, they spray down into a larger area. In the next section we discuss another contribution to a large spot size on the basis of the importance of the low-intensity wings of the laser pulse.

We also measure the total K_α production as a function of the target position with respect to the location of best focus. Using the fundamental wavelength and "no prepulse", we observed a clear maximum in each direction away from the location of best focus. At the location of maximum of K_α emission, the incident laser intensity is less than 1/10 of the value at best focus. When we measure K_α emission using the second harmonic of the laser, we see a relatively sharp maximum around the location of best focus. In Fig. 3, the measured K_α emission is given as a function of target position using the fundamental and second harmonic of the incident laser. The lack of symmetry about the location of best focus is not understood at this time. To show results for the two wavelengths in the same figure, the K_α emission using the second harmonic is multiplied by 20. The spot size measurements, presented earlier using the fundamental wavelength, are not possible when using the second harmonic because of the reduced X-ray yield.

The K_α emission is the result of laser-generated hot electrons ionizing inner-shell electrons in the solid target. The amount and location of the K_α production depends on the energies of the hot electrons. In order to obtain an estimate of the electron energies, we measure the K_α emission from layer targets. The ratio of the K_α emission from the surface layer to the emission from the buried material provides information on the energies of the electrons. Hotter electrons will ionize deeper into the target and produce relatively more K_α emission from the buried material. We place a 10-μm layer

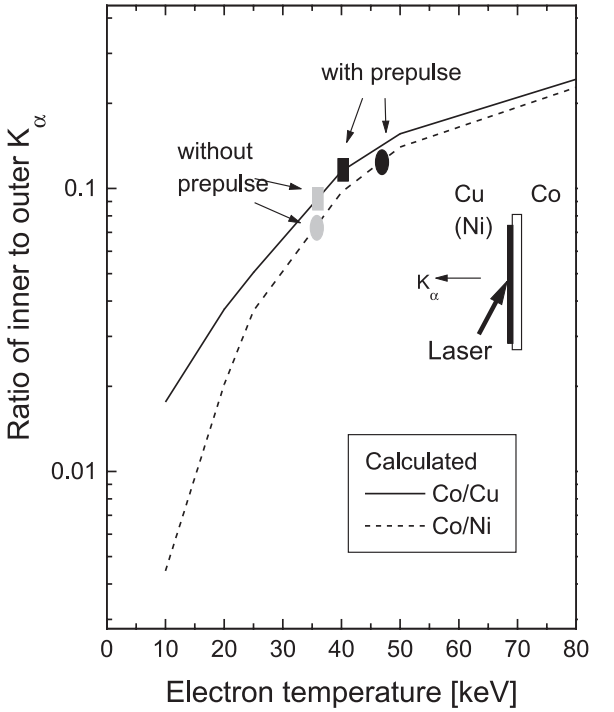

Fig. 4. Experimental ratio of Co/Cu K_α and Co/Ni K_α emission as observed from compound target with and without prepulse and the calculated ratio for these targets as a function of the electron temperature used in the simulations

of Cu or Ni over solid Co targets and measure the ratio of Co/Cu and Co/Ni K_α emission. This is done at the location of best focus with and without an applied prepulse. These data are shown in Fig. 4 along with ratios calculated with the modeling code discussed in the next section. The ratios are consistent with a hot-electron temperature of order 40 keV, with a slightly higher value for the case with a prepulse.

2 Modeling K_α production by hot electrons

We model the interaction of hot electrons with solid material using the integrated TIGER series (ITS) suite of time-independent, coupled electron/photon Monte Carlo transport codes [20]. The origin of the ITS series is the ETRAN code of Berger and Seltzer [21]. We use version 3.0 of the ITS package, which was released in 1992. There are eight codes in the ITS package, which allows one to model 1D, 2D, and 3D geometries, problems with or without specified macroscopic electric and magnetic fields, and problems extending down to energies below 10 keV. For this study, we use the CYLTRANP code, which is appropriate for problems with axial symmetry, no electric or magnetic fields, and where resolution in the 1 to 10 keV range is required. (All codes cover the 10 keV to 1 GeV range.) The ITS codes that treat the 1–10 keV range use a more elaborate ionization/relaxation model that includes K, L1, L2, L3, M, and N shells. While the materials and incident electron beam specified in CYLTRANP must have axial symmetry, the electron trajectories are fully 3D. The code tracks the electrons in the initial beam as well as all secondary electrons produced during interaction with the solid material. In contrast to the GEANT Monte Carlo code [22], which has also been used to model electron interaction with solid materials [23], the ITS codes calculate the production of characteristic radiation in addition to the bremsstrahlung radiation that both code packages calculate. The generation and transport of 8-keV Cu K_α characteristic photons calculated by the ITS code are used to help understand the interaction of a laser-generated electron beam with a Cu slab.

Since electric and magnetic fields are not included in our simulations, effects such as electron slowdown by the generated electrostatic fields or increased electron collimation due to azimuthal magnetic fields in the target material are not modelled. Such effects have been predicted (see, for example, [24]) and experimentally observed at high intensities [25, 26]. Furthermore, electric and magnetic fields generated in front of the target may result in lateral transport of suprathermal electrons along the target surface [27, 28]. For a defocused beam such effects are not expected to influence significantly the results of our experiment. Near best focus, however, the observed deviations between experiment and simulation results may be explained by electric or magnetic field effects (see Sect. 3).

The amount of K_α emission one would expect from an exponential distribution of hot electrons incident on a solid target depends on the temperature of the electrons for a number of reasons. Hotter electrons have a smaller cross section and thus produce K_α emission deeper inside the target. However, each electron has more energy and can produce a larger number of K_α photons. The number of K_α photons that escape through the front surface depends on the depth inside the target where they are produced. This is illustrated in Fig. 5, which shows the calculated number of Cu K_α photons per electron as a function of the temperature of the incident electrons (solid line). The sharp cutoff at low electron energy is because the majority of incident electrons do not have sufficient energy to ionize an inner-shell electron of Cu and thus cannot produce any Cu K_α emission. The number of photons levels off at high temperatures, and at even higher temperatures (not shown in the figure) there is a slow decrease in photons per electron because the very high energy electrons create K_α photons at a location too deep into the target to escape out the front side. The dashed line in Fig. 5 shows the number of K_α photons if the energy into electrons is kept constant. We have normalized so that the number of electrons at a temperature of 100 keV is the same. The photon numbers at lower temperatures are larger because the number of electrons increases with decreasing temperature to keep a constant amount of energy in the total hot-electron population. This curve shows that a constant laser pulse energy converted into hot electrons of different temperatures (for example by defocusing the laser, as in our experiment) results in enhanced front-side emission at a lower electron temperature.

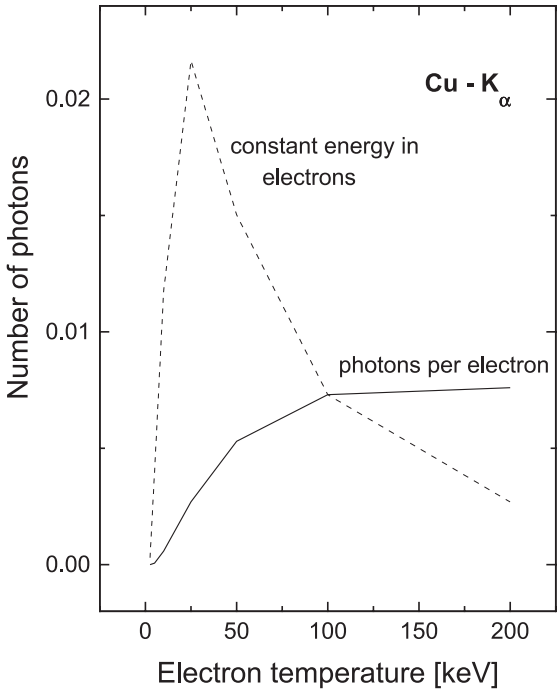

Fig. 5. *Solid line*: the calculated number of Cu K$_\alpha$ photons per number of incident electrons as a function of incident electron temperature. This number applies to the photons that escape from the front surface of a solid Cu target. *Dashed line*: number of Cu K$_\alpha$ photons as a function of incident electron temperature if the amount of energy in the hot electrons is kept constant. The number of electrons is normalized to be the same at a temperature of 100 keV. The values at lower temperatures are larger because the number of lower energy electrons increases with decreasing temperature to keep constant energy in the hot electrons

3 Analysis of experiments using the Monte Carlo electron/photon transport code

In the experiment, we observed that the FWHM of the Cu K_α emission is significantly larger than the FWHM of the inci-

dent laser intensity even for the case of "no prepulse". A possible explanation for this is associated with the low-intensity wings of the incident laser. As discussed above, there is an expected scaling of laser intensity/wavelength with electron temperature, where $T_{\rm hot}$ is proportional to $(I\lambda^2)^{1/3}$. The standard approach is to associate one electron temperature with a given pulse using an averaged intensity. We consider an alternative approach where a laser pulse produces electrons that have a radial temperature dependence that depends on the radial dependence of the laser intensity. Thus one would have the hottest electrons at the center of the laser spot surrounded by cooler electrons associated with the low-intensity wings of the laser pulse. The effect of a low-intensity wing surrounding the hot central spot has previously been invoked to explain an anomalously low apparent electron temperature in experiments with KrF laser pulses [29].

The measured radial dependence of the laser intensity at the location of best focus is shown in Fig. 6 for both the fundamental and second harmonic wavelengths. The radial dependence is seen to be similar for the two wavelengths, with the intensity at the second harmonic being about 40% of the fundamental.

For the ITS/CYLTRANP code, we specified a spot size and an energy spectrum for the incident electrons. A number of calculations are done for a given laser intensity profile where the electron spectrum is Maxwellian with a temperature that scales with the intensity to one third. The intensity is divided into four annular regions with the intensity changing a factor of 10 between the inner and outer radii of each annulus. For the fundamental wavelength, the radii where the intensity drops below 10^{18}, 10^{17}, 10^{16}, and $10^{15}\,\mathrm{W/cm^2}$ are determined. Between these radii, the electron temperature is taken as constant. From the $I^{1/3}$ scaling, the electron temperature changes by a factor of approximately 2 between two adjacent annular regions. We take the efficiency of converting laser energy into hot electrons to be independent of intensity. The code cannot model an annulus of electrons, and so we must first simulate a disk with a radius equal to the outer radius of the annulus and then subtract the results of using a disk with a radius equal to the inner radius of the annulus. The radial dependence of the laser has not been measured for target positions away from best focus. Therefore, to determine the radii where the intensity drops below 10^{18}, 10^{17}, 10^{16}, and $10^{15}\,\mathrm{W/cm^2}$, we use the focusing properties of our f/2.5 optics with an assumed Gaussian radial dependence of intensity. At different positions at and away from best focus, we calculate the FWHM of the K_α emission that escapes out the front of the Cu slab. We take the electron temperature corresponding to intensities between $10^{19}\,\mathrm{W/cm^2}$ and $10^{18}\,\mathrm{W/cm^2}$ to be 100 keV. The electron temperature at lower intensities just scales as the intensity to the one-third. These electron temperatures give results that are consistent with the measured ratio of K_α emission using layered targets. (At best focus, the percentages of the K_α emission from the four annular regions are 18%, 57%, 22%, and 3%, respectively, going from highest-intensity (10^{19}–$10^{18}\,\mathrm{W/cm^2}$) to the lowest–intensity (10^{16}–$10^{15}\,\mathrm{W/cm^2}$) annulus. The same emission would be obtained with a single-electron temperature of order 40 keV, see Fig. 4.) The calculated FWHM of the K_α emission as a function of the distance from best focus is shown in Fig. 7 for the fundamental wavelength. We also give the measured K_α emission using no prepulse and the FWHM of the laser intensity as already presented in Fig. 2. The calculated spot size of K_α emission is significantly larger than the laser spot size for positions near the best focus but still somewhat short of the measured spot size of the K_α emission. As mentioned earlier, electric or magnetic fields may be responsible for this discrepancy by adding velocity components parallel to the target surface to the electron velocity distribution. At a distance from best focus, the intensity in the wings of the profile is too low to produce significant K_α emission and the calculated spot size approaches the laser intensity spot size.

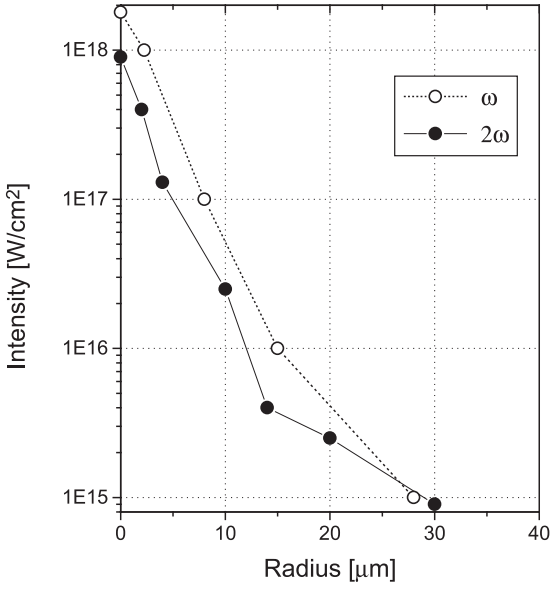

Fig. 6. The measured radial dependence of the laser intensity for the fundamental and the second harmonic of the MPQ Ti:sapphire laser focused by f/2.5 off-axis parabola

The amount of K_α emission that escapes from the front of a solid target depends on the temperature of the electrons. In Fig. 5, we showed that there is a clear maximum in Cu for an electron temperature of order 25 keV. At best focus, we determined that the appropriate electron temperature is about 40 keV. More Cu K_α emission would thus be expected if the same amount of energy is delivered to the target at a lower intensity in the $10^{16}\,\mathrm{W/cm^2}$ range. Figure 8 shows the calculated Cu K_α emission as a function of distance from best focus for both the fundamental and the second harmonic. For the fundamental wavelength, we use the same electron temperatures that are used in the calculation of the Cu K_α emission spot size. For the calculation of the total Cu K_α emission, it is not necessary to perform a series of ITS/CYLTRANP runs for each target position. One can simply use the calculated laser intensity profile and the calculated Cu K_α emission as functions of the electron temperature given in Fig. 5. From the $(I\lambda^2)^{1/3}$ scaling of the electron temperature with intensity and wavelength, we expect a factor of approximately two lower temperatures for the second harmonic. The peak of the Cu K_α emission would thus be expected to occur at or near best focus. From Fig. 8, it is seen that this is confirmed when using the second harmonic intensity profiles. It is expected that a smaller number of electrons will be produced for the second harmonic, since the very low prepulse level in this case results in a small plasma scale length which is far from optimum for efficient resonant absorption [30]. The K_α emis-

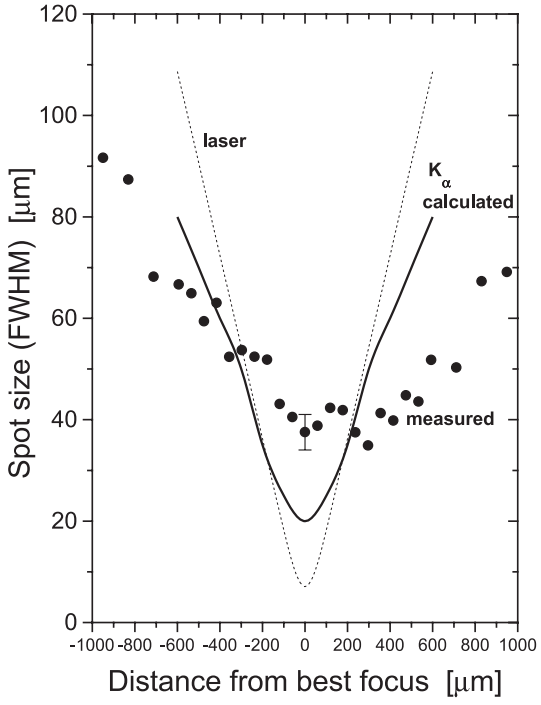

Fig. 7. The calculated FWHM of Cu K_α emission compared to experimental data for the case of "no prepulse" along with the FWHM of the incident laser intensity. As in Fig. 2, negative values of the distance indicate that the focus is in front of the target

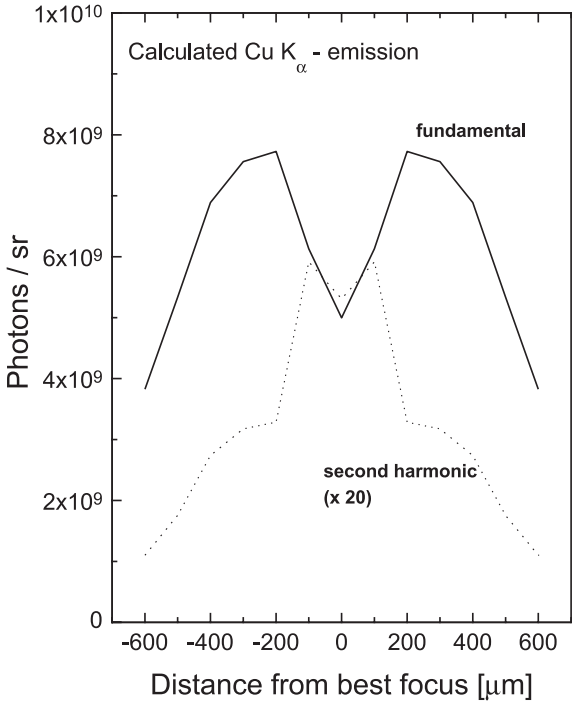

Fig. 8. The calculated amount of Cu K_α emission as a function of position away from best focus for the fundamental and second harmonic. As in Fig. 3, the second harmonic result is multiplied by a factor of 20. The normalization of the emission for the fundamental to the experimental data of Fig. 3 results in an electron energy-conversion efficiency of 15% and a total number of 1.2×10^{13} electrons at best focus. For the second harmonic the number of electrons and the conversion efficiency are reduced by a factor of 10

sion calculated for the second harmonic, with a factor of 10 fewer electrons, is found to be a factor of about 20 less than for the fundamental at best focus. As in Fig. 3, we have multiplied the second-harmonic result by this factor in Fig. 8. In comparing Fig. 8 with the experimentally measured emission in Fig. 3, it is seen that the modeling provides an explanation for the differences in the location of the target position for highest K_α emission and the ratio of emission observed at the two wavelengths.

By normalizing the theoretical K_α emission to the experimental values we arrive at a 15% efficiency of conversion into electrons with temperatures between 10 and 100 keV. The total number of such electrons is 1.2×10^{13} at best focus and increases when the laser is defocused. As mentioned earlier, the number of electrons for the data with the second harmonic is reduced by a factor of 10; the conversion efficiency into suprathermal electrons is reduced by the same factor.

4 The use of K_α emission as an X-ray laser pump source

Photons from K_α emission are an ideal pump source for inner-shell photoionization in an element with a slightly lower Z. In this case, the K_α photon from the higher Z element has enough energy to remove a K-shell electron from the lower-Z element. The cross-section for removing a K-shell electron is significantly larger than for L-shell ionization. The energy of the K_α pump photon can be very near the maximum of the K-shell cross section. The K-shell hole decays radiatively (emitting the lasing photon) or by emission of an Auger electron. The lower-laser state consists of atoms with an L-shell hole. In order to have quasi-cw inversion, it is necessary to have the L-shell holes decay faster than they are being created by radiative emission from the upper-laser state (K-shell hole). For a certain range of elements ($13 < Z < 40$) such quasi-cw operation appears to be possible [8–10]. It is critical to keep the hot electrons away from this lower-Z lasant because electrons predominantly ionize outer shells and can destroy the inversion. Even if hot electrons are kept out of the lasant, photoionized and Auger electrons can ionize the outer shells and produce an electron avalanche that limits the duration of the inversion. This effect sets an upper limit of about 100 fs to the pulse duration.

A scheme has been proposed to use K_α emission as a pump for inner-shell X-ray lasing [12]. In this scheme, the laser produces an electron beam that propagates along a thin cylinder of solid material, the converter. The hot electrons generate K_α emission that escapes out of the sides of the cylinder. The laser material, having lower nuclear charge, surrounds the converter and emits X-ray laser radiation in the direction of the electron beam. For this scheme to be successful, it is critical that the hot electrons are confined to traveling along the cylinder. Calculations using the ITS code indicate that a strong magnetic field, either self-generated or externally imposed, is needed to provide the required amount of collimation to keep them within the converter and prevent them from reaching the laser medium and destroying the inversion. Future experiments measuring the spatial dependence of K_α emission from the rear side of targets are planned. These experiments will help address the question of electron beam collimation.

5 Conclusions

We have observed that the spot size of K_α emission, generated from laser-produced hot electrons, is significantly larger than the laser spot size for target positions near best focus with and without a prepulse. The large spot with a prepulse is believed to be the result of lateral motion of hot electrons in the relatively large preplasma. When no applied prepulse is used, Monte Carlo modeling shows that a large K_α spot size can result from efficient generation of K_α emission in the low-intensity wings of the laser. When the fundamental wavelength of the laser is used, a clear maximum of K_α emission is observed at a target position away from best focus, where the peak intensity is down by more than an order of magnitude from the value at best focus. In contrast, the second harmonic of the laser produces peak K_α emission near best focus. Modeling that uses a scaling of hot electron temperature as $(I\lambda^2)^{1/3}$ is able to explain both of these observations. In addition, the reduction of K_α emission observed for the second harmonic is consistent with the modeling, where fewer and colder electrons are expected. The hot-electron temperatures used in the modeling are based on fitting our measurement of K_α emission from layer targets. Using the fundamental wavelength, with the target at best focus, we calculate that the electrons have an average temperature of order 40 keV. We discussed the use of K_α emission in photoionizing inner-shell electrons as a potential pump source for a short-wavelength X-ray laser and the importance of electrons being confined in a channel as they pass through the solid material. Planned experiments will address this issue of electron collimation by measuring the K_α emission from the rear side of solid targets using the techniques presented in this paper.

Acknowledgements. D. Eder was supported by the Alexander von Humboldt Foundation and the US DoE under LLNL Contract No, W-7405-ENG-48. This work was supported in part by the Commission of the European Communities within the framework of the Euratom/Max-Planck-Institut für Plasmaphysik Association.

References

1. P. Maine, D. Strickland, P. Bado, M. Pessot, G. Mourou: IEEE J. Quantum Electron. **QE-24**, 398 (1988)
2. G.A. Mourou, C.P.J. Barty, M.D. Perry: Phys. Today **51**, 22 (1998)
3. D. Umstadter, S.Y. Chen, A. Maksimchuk, G. Mourou, R. Wagner: Science **273**, 472 (1996)
4. Z. Jiang, J.C. Kieffer, J.P. Matte, C.Y. Cote, Y. Beaudoin, D. Gilles, G. Korn, A. Maksimchuk, S. Coe, G. Mourou, O. Peyrusse, D. Gilles: Phys. Plasmas **2**, 1702 (1995)
5. A. Rousse, P. Audebert, J.P. Geindre, F. Fallies, J.C. Gauthier, A. Mysyrowicz, G. Grillon, A. Antonetti: Phys. Rev. E **50**, 220 (1994)
6. R. Shepherd, D. Price, W. White, S. Gordan, A. Osterheld, R. Walling, W. Goldstein, R.J. Stewart: J. Quant. Spectrosc. Radiat. Transfer **51**, 357 (1994)
7. M.A. Duguay, P.M. Rentzepis: Appl. Phys. Lett. **10**, 350 (1967)
8. R.C. Elton: *X-Ray Lasers* (Academic Press, San Diego 1990) p. 107
9. Yu.L. Stankevich: Sov. Phys. Doklady **15**, 356 (1970)
10. F.T. Arecchi, G.P. Banfi, A.M. Malvezzi: Opt. Commun. **10**, 214 (1974)
11. S.J. Moon, D.C. Eder: Phys. Rev. A **57**, 1391 (1998)
12. E. Fill, D.C. Eder, K. Eidmann, J. Meyer-ter-Vehn, G. Pretzler, A. Pukhov, A. Saemann: In Proceedings of the 6th International X-Ray Laser Conference, Kyoto, Japan, 1998; Inst. Phys. Conf. Ser. No. 159, 1999, p. 301
13. A. Pukhov, J. Meyer-ter-Vehn: Phys. Plasmas **5**, 1880 (1998)
14. D.W. Forslund, J.M. Kindel, K. Lee: Phys. Rev. Lett. **39**, 284 (1977)
15. P. Gibbon, E. Förster: Plasma Phys. Controlled Fusion **38**, 769 (1996)
16. F.N. Beg, A.R. Bell, A.E. Dangor, C.N. Danson, A.P. Fews, M.E. Glinsky, B.A. Hammel, P. Lee, P.A. Norreys, M. Tatarakis: Phys. Plasmas **4**, 447 (1997)
17. J.C. Kieffer, Z. Jiang, A. Ikhlef, C.Y. Cote, O. Peyrusse: J. Opt. Soc. Am. B **13**, 132 (1996)
18. M. Zepf, G.D. Tsakiris, G. Pretzler, I. Watts, D.M. Chambers, P.A. Norreys, U. Andiel, A.E. Dangor, K. Eidmann; C. Gahn, A. Machacek, J.S. Wark, K. Witte: Phys. Rev. E **58**, R5253 (1998)
19. G. Pretzler, E.E. Fill: unpublished
20. S.M. Seltzer: Appl. Radiat. Isot. **42**, 917 (1991)
21. M.J. Berger, S.M. Seltzer: National Bureau of Standards Report 9837 (1968)
22. R. Brun et al. *Geant User's Guide*, CERN report DD/EE/82 (1982)
23. C. Gahn, G. Pretzler, A. Saemann, G. D. Tsakiris, K. J. Witte, D. Gassmann, D. Rudolph, T. Schatz, U. Schramm, P. Thirolf, D. Habs: Appl. Phys. Lett. **25**, 3662 (1998)
24. J.R. Davies, A.R. Bell, M.G. Haines, S.M. Guérin: Phys. Rev. E **56**, 7193 (1997)
25. T. Feurer, W. Theobald, R. Sauerbrey, I. Uschmann, D. Altenbernd, U. Teubner, P. Gibbon, E. Förster, G. Malka, J.L. Miquel: Phys. Rev. E **56**, 4608 (1997)
26. M. Tatarakis, J.R. Davies, P. Lee, P.A. Norreys, N.G. Kassapakis, F.N. Beg, A.R. Bell, M.G. Haines, A.E. Dangor: Phys. Rev. Lett **81**, 999 (1998)
27. D.W. Forslund, J.U. Brackbill: Phys. Rev. Lett. **48**, 1614 (1982)
28. J.M. Wallace: Phys. Rev. Lett. **55**, 707 (1985)
29. U. Teubner, I. Uschmann, P. Gibbon, D. Altenbernd, E. Förster, T. Feurer, W. Theobald, R. Sauerbrey, G. Hirst, M.H. Key, J. Lister, D. Neely: Phys. Rev. E **54**, 4167 (1996)
30. J.C. Gauthier, S. Bastiani, P. Audebert, J.P. Geindre, A. Rousse, C. Quoix, G. Grillon, A. Mysyrowicz, A. Antonetti, R. Mancini, A. Shlyaptseva: SPIE **3157**, 52 (1997)